AN EXPERIMENTAL INVESTIGATION OF THE EQUILIBRIUM INTERFACE TECHNIQUE

Thesis by

John A. Copper

In Partial Fulfillment of the Requirements

For the Degree of

Aeronautical Engineer

California Institute of Technology

Pasadena, California

1961

ACKNOWLEDGMENTS

The author wishes to express his deep appreciation to Professor Anatol Roshko for his guidance and encouragement. He would also like to thank Professors Lester Lees and E. E. Zukoski for their helpful discussions.

The Southern California Cooperative Wind Tunnel sponsored the research and the author would like to thank the many members of its staff who gave assistance, especially Mr. J. M. Spiegel and Mr. E. Pounder. Special thanks for his cooperation are due to Mr. C. M. Berdahl who designed the instrumentation.

The author wishes to thank his wife for typing the manuscript and Mr. T. Umehara and Mr. Z. Zemgals for preparing the figures.

ABSTRACT

The equilibrium interface technique has been suggested as a possible shock tunnel driver method. If this technique is workable, reservoir enthalpy levels can be increased substantially over those obtainable with the tailored interface technique without any physical modification of the shock tube. In order to determine the feasibility of the equilibrium interface technique as a shock tunnel driver method, experiments were performed in a shock tube, utilizing a cold helium driver, over the shock Mach number range 3.29 to 7.26.

Pressure histories were measured at the end of the driven tube; this pressure was found to reach an equilibrium condition for the complete shock Mach number range investigated. From the pressure histories the equilibrium pressure, time to reach equilibrium, and test time were determined. Measured equilibrium pressures were compared with an exact theory and two approximate theories. From the measured equilibrium pressure, the equilibrium enthalpy level was computed. The maximum equilibrium enthalpy was more than six times the reservoir enthalpy produced using the tailored interface technique.

TABLE OF CONTENTS

SYMBOLS

a	speed of sound
E	voltage
h	enthalpy
L	length of driven tube
M	Mach number
M_S	shock Mach number; the speed of a shock wave relative to the gas into which it is propagating divided by the speed of sound in that gas
p	static pressure
R	gas constant
s	entropy
T	static temperature
t	time
u	velocity in the x direction
x	distance downstream of the diaphragm station
γ	ratio of specific heats

Subscripts

o	standard conditions at 1 atmosphere pressure and a temperature of $273^{\circ}K$
$1,2,3...$	static conditions in the numbered region of the shock tube wave diagram
E	equilibrium state in driven gas
e	equilibrium state in driver gas

I. INTRODUCTION

A body moving at hypersonic speeds is preceded by a strong shock wave which raises the air temperature several thousand degrees. At these high temperatures dissociation and ionization of air molecules as well as excitation of their vibrational and rotational states may take place. These real gas effects influence the flow field about a body. If these real gas effects are to be studied in the laboratory it is important that enthalpy as well as Mach number be simulated.

The shock tunnel is a convenient device for producing both the high enthalpy levels and high Mach numbers associated with hypersonic flight. Shock tunnels use a shock tube to process the test gas to a high enthalpy state. One of the simplest methods is to allow the incident shock wave to reflect from the downstream end of the shock tube, creating a region of stagnant, compressed, high-temperature gas, which is then used to supply the nozzle. The state of this gas, in thermal equilibrium, can be calculated quite precisely from the normal shock relations.

An inherent limitation of the shock tunnel is the short time duration of steady flow. Here the testing time (time of constant reservoir conditions)

is limited to the time it takes for the reflected shock wave to reflect off the interface separating the driver and driven gases and return to the downstream end of the tube. This time, $t_B - t_A$ in Fig. 1, is directly proportional to the driven tube length. In order to provide adequate testing time, shock tubes had to be made quite long. This led to considerable shock wave attenuation (Ref. 1) resulting in unsteady reservoir conditions.

Under certain conditions the reflected shock wave can be passed through the interface without reflection. This method is called the tailored interface technique (Ref. 2), and it increases the testing time by an order of magnitude. However, if the state and composition of the driver and driven gases are specified, tailoring is theoretically possible for only one incident shock strength. For example, if the driver and driven gases are helium and air, each at room temperature, the tailoring shock Mach number is about 3.5. To tailor at higher shock Mach numbers the driver gas must be heated, either by combustion (Ref. 3), electric arc discharge (Ref. 3), or slow electric heating (Ref. 4).

The equilibrium interface technique was suggested by Hertzberg (Ref. 5) as another possible driver

technique. Here the additional shock reflections between the interface and the end of the tube are allowed to occur; they become successively weaker until the interface is brought to rest and an equilibrium condition is reached (Fig. 1). Tailoring is the special case where equilibrium is reached after one shock reflection. Higher reservoir enthalpy levels are possible than with the tailored interface technique, since the incident shock wave can in general be stronger than required for tailoring; furthermore, the additional reflections also increase the enthalpy level. Thus the equilibrium interface technique offers increased performance over the tailored interface technique while possibly retaining some of its test time advantages.

II. THEORETICAL ANALYSIS

It will be of interest to try to predict theoretically from the shock tube initial conditions the pressure and temperature of the gas in the equilibrium state (p_E and T_E). While the pressure can be measured directly in an experiment, the temperature must be calculated from other measured quantities. Also, the time duration that the equilibrium condition persists ($t_F - t_E$ in Fig. 1) is of interest since it determines the test time.

Ideal shock tube theory is well known and has been discussed by many authors (Refs. 6, 7 and others). On the basis of this theory the flow at any time in a shock tube can be calculated (in principle) if the shock tube initial conditions are known. Some of the assumptions are:

1. The diaphragm is removed and the shock wave is formed instantaneously.
2. A plane discontinuity (interface) separates the driver and driven gases.
3. Effects of viscosity and heat conduction can be neglected.

Experimental evidence indicates that these assumptions are violated in the shock tube. For example, the driver and driven gases are separated by a constant pressure mixing region of finite width. This region, ideally the interface, is found to follow the incident shock wave more closely than the ideal theory predicts. However to

include the non-ideal effects in a shock tube theory would be extremely difficult. The ideal theory should give results that are substantially correct; therefore the non-ideal effects will be neglected in the subsequent analysis. However any results certainly will have to be verified by experiment.

By constructing a wave diagram solution the gas properties in the shock tube can be determined at any time. This construction is essentially a numerical integration using the method of characteristics (Ref. 8), and is exact under the assumptions listed above. For simplicity in constructing the wave diagram, perfect gas theory is used.

Referring to Fig. 1 for notation, this method proceeds as follows:

1. Given p_1, p_4, T_1, T_4, and the gas compositions; M_{S_1} can be calculated. Next the incident shock wave, the interface, and the expansion fans can be laid out in the x - t plane.
2. The reflected shock strength is determined by the condition $u_5 = 0$. It can be calculated and laid out to the point where it intersects the interface.
3. The strength of the waves produced by the reflected shock-interface interaction must be calculated by iteration, using the known relations $u_6 = u_7$ and $p_6 = p_7$. The state of the gas in regions

2, 3, and 5 is also known. In the p-u diagram (Sketch (a)), region 6 lies along AB, region 7 lies along CD. To find the point (6,7) where AB and CD intersect, guess p_6/p_5 and compute p_7/p_3 using $u_7 = u_5$. If $p_7/p_3 \neq p_6/p_2$ then guess again for p_6/p_5 until $p_6/p_2 = p_7/p_3$.

4. The re-reflected shock speed is calculated from p_6/p_5, and it is laid out in the x-t diagram to the point where it reaches the wall.

5. Steps 2, 3, and 4 are repeated until the equilibrium condition (E) is reached at time t_E on the x-t diagram. This condition occurs when the wave reflected downstream from the interface is of negligible strength. Usually about four or five reflections are required to reach E.

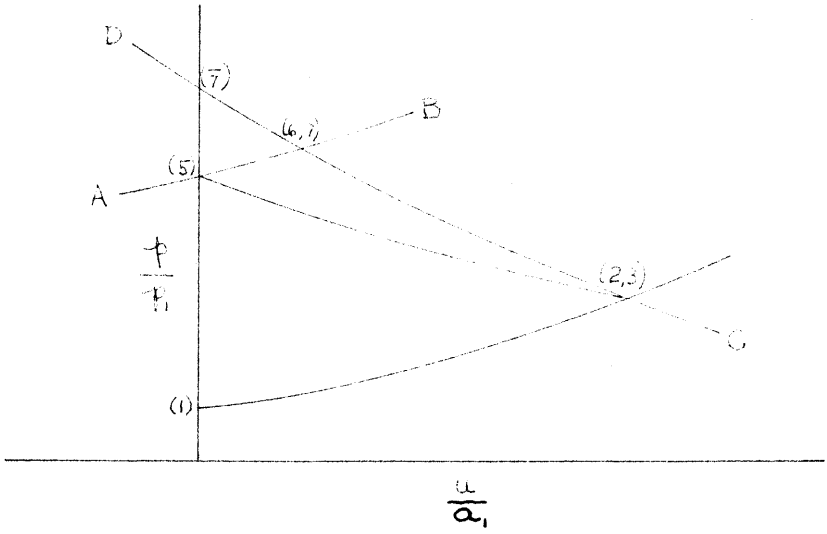

Sketch (a) p-u Diagram

The processed gas will remain stagnant until some disturbance reaches the interface from upstream. For usual shock tube geometries the disturbance arriving first results from the interaction of the reflected shock wave and the expansion wave swept downstream from the diaphragm station. This disturbance determines the theoretical test time, $t_F - t_E$ in Fig. 1.

Thus the wave diagram method enables calculation of p_E, T_E, and $t_F - t_E$, which are the desired parameters. However, the calculation is tedious and must be repeated for all gas combinations and values of M_{S_1} that are of interest.

An examination of a wave diagram solution shows that the waves reflected from the interface diminish in strength quite rapidly. This observation suggests that assuming the flow to be isentropic after the first shock wave-interface interaction may be a good approximation. If the amount of isentropic compression is known then the equilibrium temperature can be calculated. Reference 5 suggests that the equilibrium pressure is approximately the pressure that is reached if the driver gas is brought to rest by a single shock wave. Thus p_E is approximately $\bar{p}_7$ on the p-u diagram (Sketch (a)). Then

$$\frac{p_E}{p_5} = \frac{p_E}{p_3}\,\frac{p_2}{p_5} \simeq \frac{\bar{p}_7}{p_3}\,\frac{p_2}{p_5} \qquad (1)$$

where $\bar{p}_7/p_3$ is found from

$$\frac{\bar{p}_7}{p_3} = 1 + \frac{2\gamma_4}{\gamma_4+1}\left(\bar{M}_{s_3}^2 - 1\right) \qquad (2)$$

Now $\bar{M}_{s_3}$ is the value of M_{s_3} obtained by putting $u_7 = 0$ in

$$\frac{u_3 - u_7}{a_3} = \frac{2}{\gamma_4+1}\left(\frac{M_{s_3}^2 - 1}{M_{s_3}}\right) \qquad (3)$$

so that

$$\bar{M}_{s_3} = \frac{\gamma_4+1}{2} M_3 + \sqrt{\left(\frac{\gamma_4+1}{2} M_3\right)^2 + 1} \qquad (4)$$

A method suggested by Prof. A. Roshko essentially makes a linear approximation for u_7. The pressure is calculated by assuming isentropic compression from 7 to e. If the flow from 7 to e is assumed to be isentropic and through a simple wave, then the Riemann variable $\left[2/(\gamma-1)\right] a + u$ is conserved. Since $u_e = 0$,

$$\frac{2}{\gamma_4 - 1} a_7 + u_7 = \frac{2}{\gamma_4 - 1} a_e$$

$$\frac{a_e}{a_7} = 1 + \frac{\gamma_4 - 1}{2} M_7$$

and for isentropic flow

$$\frac{p_e}{p_7} = \left(\frac{a_e}{a_7}\right)^{\frac{2\gamma_4}{\gamma_4 - 1}}$$

so that

$$\frac{p_e}{p_7} = \left(1 + \frac{\gamma_4 - 1}{2} M_7\right)^{\frac{2\gamma_4}{\gamma_4 - 1}} \qquad (5)$$

Now

$$M_7 = \frac{u_7}{a_7} = \frac{u_7/a_3}{a_7/a_3}$$

where

$$\frac{a_7}{a_3} = \frac{\left[2\gamma_4 M_{s_3}^2 - (\gamma_4 - 1)\right]^{1/2}\left[2 + (\gamma_4 - 1) M_{s_3}^2\right]^{1/2}}{(\gamma_4 + 1) M_{s_3}} \tag{6}$$

and

$$\frac{u_7}{a_3} = M_3 - \frac{2}{\gamma_4 + 1}\,\frac{M_{s_3}^2 - 1}{M_{s_3}} \tag{7}$$

To find M_{s_3} assume that

$$M_{s_3} = \bar{M}_{s_3}(1 + \epsilon)$$

where $\epsilon << 1$ and $\bar{M}_{s_3}$ is value of M_{s_3} computed from equation 4 (assuming $u_7 = 0$). Then

$$M_{s_3}^2 \simeq \bar{M}_{s_3}^2 (1 + 2\epsilon)$$

$$\frac{p_7}{p_3} = 1 + \frac{2\gamma_4}{\gamma_4 + 1}\left(M_{s_3}^2 - 1\right) = 1 + \frac{2\gamma_4}{\gamma_4 + 1}\left(\bar{M}_{s_3}^2 - 1\right) + \frac{4\gamma_4 \epsilon \bar{M}_{s_3}^2}{\gamma_4 + 1}$$

$$\frac{p_7}{p_3} = \frac{\bar{p}_7}{\bar{p}_3} + \frac{4\gamma_4 \epsilon \bar{M}_{s_3}^2}{\gamma_4 + 1}$$

To determine ϵ, use

$$\frac{u_7}{a_3} = M_3 - \frac{2}{\gamma_4 + 1}\,\frac{M_{s_3}^2 - 1}{M_{s_3}} = M_3 - \frac{2}{\gamma_4 + 1}\left[\frac{\bar{M}_{s_3}^2 - 1 + 2\epsilon \bar{M}_{s_3}^2}{(1 + \epsilon)\bar{M}_{s_3}}\right]$$

$$\frac{u_7}{a_3} = \left(M_3 - \frac{2}{\gamma_4 + 1}\,\frac{\bar{M}_{s_3}^2 - 1}{\bar{M}_{s_3}}\right) - \frac{2}{\gamma_4 + 1}\,\frac{\bar{M}_{s_3}^2 + 1}{\bar{M}_{s_3}}\,\epsilon$$

since the first term is zero by the definition of $\bar{M}_{s_3}$,

$$\epsilon = -\frac{\gamma_4+1}{2}\frac{u_7}{a_3}\frac{\bar{M}_{s_3}}{\bar{M}_{s_3}^2+1}$$

and

$$\frac{p_7}{p_3} - \frac{\bar{p}_7}{p_3} = -2\gamma_4\frac{u_7}{a_3}\frac{\bar{M}_{s_3}^3}{\bar{M}_{s_3}^2+1} \qquad (8)$$

If the wave separating regions 6 and 5 is a shock wave then

$$\frac{u_6-u_5}{a_5} = \frac{u_6}{a_5} = \frac{2}{\gamma_5+1}\left(\frac{M_{s_5}^2-1}{M_{s_6}}\right)$$

$$\frac{p_6}{p_5} = 1 + \frac{2\gamma_5}{\gamma_5+1}\left(M_{s_5}^2-1\right)$$

so that

$$\frac{u_6}{a_5} = \frac{\frac{1}{\gamma_5}\left(\frac{p_6}{p_5}-1\right)}{\left[1+\frac{\gamma_5+1}{2\gamma_5}\left(\frac{p_6}{p_5}-1\right)\right]^{1/2}}$$

Now if $\left(\frac{p_6}{p_5}-1\right) << 1$, then

$$\frac{u_6}{a_5} = \frac{1}{\gamma_5}\left(\frac{p_6}{p_5}-1\right) - \frac{\gamma_5+1}{4\gamma_5^2}\left(\frac{p_6}{p_5}-1\right)^2$$

Using this in equation 8 leads to

$$\frac{p_6}{p_5} = \frac{p_7}{p_5} = \frac{\frac{\bar{p}_7}{p_3}+\alpha}{\frac{p_5}{p_2}+\alpha} \qquad (9)$$

where

$$\alpha = \frac{2\gamma_4 a_5 \bar{M}_{s_3}^3}{\gamma_5 a_3\left(\bar{M}_{s_3}^2+1\right)}$$

Now M_{s_3} can be calculated from

$$M_{s_3}^2 = 1 + \frac{\gamma_4+1}{2\gamma_4}\left(\frac{p_7}{p_5}\frac{p_5}{p_2}-1\right) \qquad (10)$$

When p_E calculated from equations 1, 2, and 4 is compared with p_E calculated from equations 4 through 10, the results are found to differ by less than 1 per cent. Thus the assumptions: 1) p_E is the same as the pressure that is reached if the driver gas is brought to rest by a single shock wave; and 2) the compression is isentropic from 7 to e, where u_7 is found by a linear approximation; give essentially identical equilibrium pressures.

For greater accuracy, the values of u_7 and M_{S_3} can be computed exactly by the method of characteristics and then p_E can be calculated from equations 5, 6, and 7. This method will give p_E to within 1 per cent of the exact value obtained by carrying out the complete characteristics solution.

It should be noticed that the approximate theories give no information about the time it takes to reach equilibrium or the length of time the equilibrium condition persists. This information can be obtained theoretically only by constructing a wave diagram.

The preceding theories can be expected to give a rough estimate of the performance of the equilibrium interface technique. However, in light of the assumptions made it is necessary to verify experimentally that an equilibrium condition is reached. For perhaps when conditions depart too far from tailoring the impedance mismatch between the reflected shock and the interface will be too large, and no equilibrium condition will be reached

before disturbances arrive from upstream in the shock tube.

Also it is well known (Ref. 9, for example) that the incident shock strength, M_{S_1}, cannot be reliably predicted from the shock tube initial conditions. M_{S_1} is the basic parameter from which all of the properties of the flow behind the incident shock and first reflected shock are calculated. However, whether M_{S_1} can reliably predict p_E will have to be determined experimentally.

Mark (Ref. 10) has noticed that the reflected shock wave interacts with the boundary layer and in some instances separates it. This may affect the approach to equilibrium or the steadiness of the equilibrium flow.

For these reasons the feasibility of the equilibrium interface as a shock tunnel driver technique can be established only experimentally. The purpose of the experiment will be to accomplish the following: 1) Determine the range of M_{S_1} over which an equilibrium condition can be reached. 2) Obtain a measure of the uniformity of the pressure while the equilibrium condition is maintained. 3) Measure the equilibrium pressure to provide a basis for calculation of the equilibrium temperature. 4) Measure the time it takes to reach the equilibrium condition and the time the equilibrium condition persists. 5) Investigate any effects of initial pressure level.

III. DESCRIPTION OF THE EXPERIMENT

A. Shock Tube and Related Operating Equipment

The experiments were performed in the shock tube at the Southern California Cooperative Wind Tunnel*. This shock tube is of the conventional type, utilizing a compressed gas driver, and is shown schematically in Fig. 2. Room temperature helium was used exclusively as the driver gas and either air or argon was used for the driven gas. The shock tube could be operated up to 30,000 psi, although pumping facilities limited operation to under 6,000 psi.

The shock tube structure may be divided into three parts: 1) driver tube; 2) driven tube; 3) coupling nut.

The driver tube is a 3 inch I.D., 6 inch O.D. circular steel tube which is 12 feet long. The tube is sealed at one end by a blind flange and at the other by a metal diaphragm. Ports are available for gas inlet and blow-off and pressure and temperature measurements.

The driven tube is a 4-1/8 inch O.D., 2-1/8 inch I.D. circular steel tube which is 12 feet long. It is sealed at the downstream end with a blind flange and at the other end by the diaphragm. The blind

---

* Since dismantled.

flange has two ports for pressure or temperature instrumentation. Various ports are available in the tube for gas inlet and instrumentation. Specifically, ports 9.0 and 10.0 feet from the diaphragm station were fitted with thin-film resistance thermometers suitable for shock wave detection.

The coupling nut fastens the driver and driven tubes together so that the diaphragm is clamped between them. The tube end faces are smoothly machined and fitted with neoprene "O" rings so they will seal tightly against the metal diaphragm. Diaphragms of aluminum, copper, and cold-rolled steel were used in thicknesses between .012 and .103 inch. A cross-shaped scribe mark was made with a pre-set scribing tool and the diaphragms were broken by gas pressure.

Helium, the driver gas, was obtained commercially in high-pressure bottles at about 2200 psi. A booster pump, Sprauge Engineering Corp. Model S-3600 WB, could be used to raise the driver gas pressure to about 6000 psi. Driver initial pressures below 1000 psi were measured on a 0-1000 psi Marsh Mastergage to an accuracy of $\pm$ 20 psi. For higher pressures a Marsh 8000 psi gage was used; the accuracy when using it was about $\pm$ 50 psi.

Either air or argon at room temperature was used as the driven gas. The driven tube was first evacuated

with a Welch vacuum pump and then the driven gas was admitted from a commercial bottle. Nominal initial pressures of 1, 5, and 25 psia were measured with a mercury micro-manometer, referenced to the atmosphere, to an accuracy of within 1 per cent.

B. Instrumentation

Instrumentation was developed to measure: 1) the incident shock wave speed; 2) the static pressure at the downstream end of the driven tube. A block diagram of the instrumentation is shown in Fig. 3.

1. Shock Wave Speed Measurement

An average shock wave speed was determined by measuring the shock transit time between stations 9.0 and 10.0 feet from the diaphragm station. The distance between these two stations was known to $\pm$ .005 inch. Thin-film platinum resistance thermometers, similar to those described in Ref. 11, mounted flush in the driven tube were used to detect the passage of the shock wave. The signals from these gages were fed through an amplifier to the "start" and "stop" channels of a Berkeley Model 7360 counter. This counter has a resolution time of 1 μ sec. so the shock wave speed is measured to 1 per cent accuracy. The output from one of the amplifiers was also used to start the recording oscilloscopes.

2. Pressure Instrumentation

Several "home-made" piezoelectric pressure transducers were tried in the shock tube. The most satisfactory one is shown schematically in Fig. 4.

The first gage tried employed an aluminum cap (Fig. 4) with a back to front side area ratio of 16. This design reduced the pressure on the lead zirconate crystal by a factor of 16 so the gage output would be compatible with the oscilloscope for high pressures. This gage exhibited excessive overshoot and subsequent ringing. Various types of recessed mountings and shock mountings were unsuccessful in eliminating these undesirable effects. Also, it was not possible to obtain a reliable calibration of this gage.

The gage that was finally used had a quartz crystal and did not use the cap to reduce the pressure on the crystal. This gage exhibited considerably less ringing than the previous gage and was successfully calibrated. It is not known whether or not the pressure reducing cap was responsible for the difficulties encountered with the first gage.

The output from the pressure transducer was circuited through a differential cathode follower to one of the recording oscilloscopes (Tektronix 551 or 545A) and was recorded with a polaroid camera. During

calibration of the pressure gage the response time of the cathode follower increased to about 250 μ sec. This difficulty could not be remedied in the time remaining to perform the experiments so it was decided to tolerate this "long" response time since most of the times of interest were sufficiently longer than 250 μ sec. Although the output from a step input was rounded off, the time to reach 50 per cent of the full deflection was about 25 μ sec. Thus, for example, it was felt that it was poseible to distinguish qualitatively between two shock waves and one shock wave of the same total strength if the two waves were at least 25 μ sec. apart.

Under a constant load the output of the pressure measuring system decayed exponentially with time. Over a 10 m sec. time period (which was the length of the usual oscilloscope trace) the output decayed about 6 per cent; the decay was barely discernible over the final 5 m sec. period.

The pressure transducer was dynamically calibrated in the shock tube at regular intervals by comparing its output with pressures of known intensity. The known pressures were obtained by generating low strength shock waves, $1.4 \leq M_{s_1} \leq 2.0$, which obey the normal shock relations quite well. The known pressures were

calculated from the measured M_{s_1} and p_1 and theoretical values of p_5/p_1. A typical pressure calibration is shown in Fig. 5.

C. Test Program

Experiments were performed over the widest possible incident shock Mach number range at initial pressures of 1, 5, and 25 psi. The shock Mach number range was limited by the maximum and minimum driver pressures available.

Three oscilloscope channels were available to record data. One of these was always used to record a pressure history at the downstream end of the driven tube. The output of a thin-film resistance thermometer mounted in the blind flange at the downstream end of the driven tube was recorded on some runs. It was hoped that this would give some information about the uniformity of the gas temperature. It was not possible to draw any conclusions from these temperature records. On other runs a crude check on shock wave attenuation was made by comparing the shock wave transit time between stations 9.0 and 10.0 with the transit time between stations 9.0 and 12.0. No shock wave attenuation was noticeable from these measurements.

In addition, several runs were made using argon as the driven gas. Mark (Ref. 10) concluded that the

interaction between the reflected shock wave and the laminar boundary layer on the tube walls should be very weak when a monatomic driven gas is used. Experiments verified this conclusion. Thus any effects of the shock wave-boundary layer interaction should be modified when a monatomic driven gas is used.

D. Data Reduction and Accuracy

The shock Mach number M_{s_1} is computed from the measured shock speed divided by the driven gas sound speed at temperature T_1. The total error resulting from the uncertainty in the measuring interval, counter resolution, and gas initial temperature uncertainty is within 1 per cent.

Pressures are determined by measuring the oscillogram deflection, converting this to a voltage change, and then determining the pressure from the gage calibration. Errors are introduced in reading the oscilloscope trace and from the gage calibration. The method of gage calibration (Section III.B.2.) made it difficult to obtain calibration points for large pressure differences. There were only 6 points for pressure differences between 1500 and 3000 psi and no points above 3000 psi. Therefore the calibration curve had to be extrapolated above 3000 psi. Because of these factors, uncertainties in some of the measured pressures may be of the order of 10 per cent.

It was desired to present the equilibrium pressure data as p_E/p_5 vs M_{S_1} in accordance with the previously discussed theories. At the lower values of M_{S_1} (Figs. 6(a) - 6(c)) p_5 is easily determined from the pressure trace. At higher shock strengths (Figs. 6(d) - 6(h)) it became more difficult to determine p_5 accurately from the oscillograms because of the "long" response time of the pressure measuring system, the short time duration of state 5, and the relatively small deflection on the oscillogram. Therefore at the higher shock strengths p_5 is computed from the measured p_1 and M_{S_1} and the theoretical value of p_5/p_1.

The equilibrium pressure, p_E, was also determined in a rather arbitrary fashion. An examination of Fig. 6 shows that the pressure does not reach a perfectly constant value on all runs. In fact a slight pressure variation is noticed even in the run that corresponds most closely to the tailored condition (Fig. 6(b)). On some runs a greater amount of judgement had to be used to determine if an equilibrium condition was reached and where it was first reached. It was assumed that an equilibrium condition was reached at t_E if the pressure did not vary by more than 5 per cent until the test time was terminated. The character of the pressure variation over the equilibrium interval varies from run to run but a trend was noticed with M_{S_1}.

Near tailoring (Figs. 6(a) - 6(c)) the pressure increases slightly and then falls off. For higher values of M_{S_1} (Figs. 6(d) - 6(g)) the pressure either increases slightly or remains constant. At even higher shock strengths (Fig. 6(h)) the pressure increases slightly.

The time to reach equilibrium, $t_E - t_A$, and the run time, $t_G - t_E$, are measured directly from the pressure oscillograms. t_A is the point where the trace first rises, and the point where the pressure trace first becomes flat is regarded as t_E. The end of the equilibrium period is defined as t_G, the point where the pressure trace falls off noticeably. The point t_E is difficult to determine from the pressure trace since the approach to equilibrium is quite gradual. For this reason and because of the parallax associated with the oscillogram record, the uncertainty in the measured values of $t_E - t_A$ and $t_G - t_E$ is about $\pm$ 100 μsec.

IV. RESULTS AND DISCUSSION

A. Equilibrium Pressure

Data were recorded for shock Mach numbers in the range $3.29 \leq M_{S_1} \leq 7.26$ and tailoring ($p_E/p_5 = 1$) was observed near $M_{S_1} = 3.65$, as predicted by ideal shock tube theory. The results from the theoretical and experimental evaluation of p_E/p_5 as a function of M_{S_1} are shown in Fig. 8. The solid line is the locus of wave diagram solutions, exact for a perfect gas. The dashed curve represents both approximate theories discussed in Section II., which were found to give essentially identical results. The data do not agree consistently with any of the theories; in fact the scatter of the data indicates that M_{S_1} does not uniquely determine p_E.

The explanation for this behavior is related to the well known fact that shock tube flow is not ideal and experimental values of p_4/p_1 usually differ significantly from theoretical ones based on the measured M_{S_1}. Figure 9 shows how p_4/p_1 correlates with M_{S_1} for the data presented in Fig. 8. The points that are appreciably above the theoretical curves on Fig. 8 correspond to the ones that are considerably above the theoretical curve on Fig. 9. It seems that, in fact,

p_E correlates much better with the driver initial pressure, p_4, than with the theoretical curve for an ideal shock tube. This correlation is depicted in Fig. 10 where it may be seen that p_E/p_4 is nearly constant, and that the scatter is considerably less than in Fig. 8. Thus p_E is found to depend strongly on p_4.

Since the pressure over the equilibrium interval is rarely perfectly constant, the magnitude of the pressure variation is of interest. A measure of the constancy of the equilibrium pressure over the equilibrium interval is $\Delta p/p_E$, where p_E is measured at the point where the equilibrium condition is first reached, and Δp is the maximum pressure difference over the interval. Figure 11 shows how $\Delta p/p_E$ varies with M_{s_1}. It is seen that at the lower shock strengths the equilibrium pressure variation is about 4 per cent, and for shock Mach numbers greater than about 4.5 the equilibrium pressure variation is about 2 per cent.

B. Time to Reach Equilibrium and Test Time

The time to reach equilibrium is defined as $t_E - t_A$ (Fig. 1). Measured values of $(t_E - t_A)/L$ are presented in Fig. 12 as a function of p_E/p_5, which is a measure of the departure from tailoring. It is encouraging to note that for p_E/p_5 greater than about 2, the time to reach equilibrium remains nearly constant.

Theoretically, the test time is limited by the arrival (t_p) of the disturbance resulting from the interaction of the reflected shock wave and the upstream propagating expansion fan which is swept downstream from the diaphragm station (Fig. 1). The strength of this disturbance, p_8/p_7, can be calculated using the method of characteristics; for the particular shock tube geometry and gases used it turns out to be very weak. For the majority of the Mach number range of interest this disturbance is a very weak compression wave.

Figure 13 shows a wave diagram solution superimposed on a pressure oscillogram. The wave diagram solution is stopped with the arrival of the above mentioned disturbance. Two things can be noticed by comparing the theoretical and actual pressure traces: 1) The observed time to reach equilibrium is considerably longer than the wave diagram predicts. Also, no discrete shock waves are observed and the process seems more like a smooth compression. 2) The disturbance mentioned is not discernible on the pressure trace. Certainly it does not end the test time, since the equilibrium condition is not reached until well after the predicted arrival of this disturbance. This conclusion cannot be extended to arbitrary shock tube geometries and gas combinations. For example Holder

and Schultz report (Ref. 12) that this disturbance is important for the shock tube configuration they used (hydrogen driver gas, no area change at the diaphragm section).

For the reasons mentioned above, the test time ends with the arrival (t_G) of the head of the expansion wave, which has been reflected off the driver tube end wall. The test time is defined as $t_G - t_E$, and measured values of $(t_G - t_E)/L$ are presented in Fig. 14 as a function of p_E/p_5. These results appear to be more scattered than the results presented in Fig. 12. This scatter is caused by the variation (for a given p_E/p_5) in the time of arrival of the reflected head of the expansion wave, which defines t_G.

C. Miscellaneous Gasdynamical Considerations

1. Initial Pressure Level

No effect of initial pressure level was noticed in the equilibrium pressure ratio, time to reach equilibrium, or test time results. The initial pressures are typical of those that would be used in a shock tunnel for Reynolds number as well as Mach number and enthalpy simulation for typical re-entry bodies, and are high enough so that initial pressure effects apparently are not important.

2. Reflected Shock Wave-Boundary Layer Interaction

Mark (Ref. 10) has observed that the low energy portion of the laminar boundary layer on the tube walls cannot pass through the reflected shock wave without separating. This phenomenon could alter the process of coming to equilibrium and the steadiness of the equilibrium period. The interaction effect is diminished when the boundary layer becomes turbulent, since energy is transferred into the low energy portion of the boundary layer. At the Cornell Aeronautical Laboratory, no effects of the shock-boundary layer interaction have been found in the air processed in their tailored-interface shock tunnel, which operates at high pressures (Ref. 2). In the present experiments, the boundary layer behind the incident shock wave became turbulent almost immediately and the interaction effect is not expected to be significant.

However Holder and Schultz (Ref. 12) have noticed that the pressure measured near the shock tube end falls immediately after the reflection of the incident shock wave. They attribute this behavior to the attenuation of the reflected shock wave resulting from the interaction with the boundary layer. This effect could be noticed in the present experiment at the lower shock strengths (Figs. 6(a) - 6(c)). When argon was used

for the driven gas this effect was not noticed, in fact there was an unexpected rise in pressure at the lower shock strengths (Figs. 7(a), 7(b)). It is possible that these phenomena can be attributed to the reflected shock-boundary layer interaction.

3. Effect of a Monatomic Driven Gas

Several runs were made using argon as the driven gas. Qualitatively the results were similar to those obtained with air, except for the unexpected rise in pressure discussed in the previous section. A quantitative comparison of pressure data was not possible because some technical difficulties arose which made it impossible to obtain an accurate pressure calibration for these runs.

4. Actual Process to Equilibrium

It was noted in a previous section that the approach to equilibrium is not by a series of discrete shock waves, decreasing in strength, as a wave diagram solution would predict. Instead the pressure increases in a rather smooth fashion; the compression is gradual not discontinuous.

The absence of discrete shock waves can be explained by considering the shock wave-interface interaction.

To fix ideas, consider the case where the incident shock wave is stronger than required for tailoring. The entering reflected shock will be weaker than the transmitted shock ($p_7/p_3 > p_5/p_2$). If the interface is a sharp discontinuity the re-reflected wave will be a shock wave as illustrated in Fig. 15(a). Actually a constant pressure mixing region of finite width separates the driver and driven gases (Fig. 15(b)). The entering reflected shock wave gradually increases in strength as it passes through this region and the re-reflected disturbance consists of a family of converging characteristics which form a weak shock wave when they merge. For practical purposes, weak shock waves ($p_2/p_1 < 1.2$) can be considered to be isentropic since $(s_2 - s_1)/\gamma R < .001$. For these reasons, the process between states 5 and E can be considered to be isentropic or nearly so.

It is also interesting to note that if isentropic compression is assumed from state 3 to e, then for a constant area tube the driver gas undergoes isentropic expansion through a simple wave to u_3 and then is compressed isentropically through a simple wave to state e. For this process, $p_e = p_4$ for any value of M_{s_1}. This is approximately the result presented in Fig. 10.

D. Equilibrium Temperature and Enthalpy Levels

Before the equilibrium temperature and enthalpy can be computed, some assumption must be made about the process between states 5 and E. On the basis of the discussion in Section IV. C. 4. the flow is assumed to be isentropic between states 5 and E. The calculation of the state of the gas in the equilibrium condition proceeds as follows: 1) p_5 and T_5 are determined from the normal shock relations and the measured values of p_1, T_1, and M_{s_1}. 2) State 5 (p_5, T_5) is located on a Mollier diagram. 3) State E is found by following an isentrope from state 5 until the measured pressure p_E is reached. Thus M_{s_1} and p_E/p_5 (along with p_1 and T_1) completely determine the state of the equilibrium gas.

The maximum equilibrium temperature computed by this method was 6300°K corresponding to $h_E/RT_o = 138.5$. These values were obtained at $M_{s_1} = 7.26$ where $T_5 = 4415°K$ and $h_5/RT_o = 90.2$. It should be noted that for this case the additional shock reflections increased the temperature nearly 1900°K. The tailored interface technique can be used at $M_{s_1} = 3.65$; the reservoir enthalpy level corresponding to tailoring is $h_5/RT_o = h_E/RT_o = 22.7$. Thus by using the equilibrium interface technique the reservoir enthalpy level can be increased to many times the tailored value.

E. Shock Tunnel Performance

The shock tunnel reservoir enthalpy can be associated with stagnation enthalpy simulation at a flight Mach number if the ambient temperature is specified. Picking 218°K as the ambient temperature (altitudes between 35,000 and 105,000 feet) then the maximum equilibrium enthalpy, $h_E/RT_o = 138.5$, corresponds to a flight Mach number of 16.4.

Using the tailored interface technique (with a cold helium driver gas), stagnation enthalpy can be simulated at a flight Mach number of 6.35. Thus these experiments show that the maximum shock tunnel Mach number for stagnation enthalpy simulation can be increased from 6.35 to at least 16.4 by using the equilibrium interface technique. This increase in performance is attained with a decrease in the test time of about 70 per cent. Even greater performance gains should be possible if larger values of p_4/p_1 are used.

The shock Mach number for tailoring can be increased by using either hydrogen or heated helium as the driver gas. If comparable performance gains can be achieved by using the equilibrium interface technique with these driver gases, enthalpy simulation should be possible up to satellite velocities.

V. SUMMARY AND CONCLUSIONS

The feasibility of the equilibrium interface technique as a shock tunnel driver method was investigated by measuring pressure histories at the downstream end of a shock tube utilizing a cold helium driver. Measured pressures reached an equilibrium condition for the entire shock Mach number range investigated, i.e. for $3.29 \leq M_{s_1} \leq 7.26$. The equilibrium enthalpy calculated at $M_{s_1} = 7.26$ was more than six times the enthalpy corresponding to tailoring, which occurs at $M_{s_1} = 3.65$.

The measured equilibrium pressures do not correlate with M_{s_1} as the exact and approximate shock tube theories predict. Instead a strong dependence on the driver initial pressure was found; the equilibrium pressure was about 1.1 times the driver pressure for all values of M_{s_1} investigated.

As conditions depart from tailoring, the time to reach equilibrium increases; however for p_4/p_5 greater than about two, this time remains nearly constant. The test time decreases as conditions depart from tailoring, falling to about 30 per cent of the tailored test time at $M_{s_1} = 7.26$. This test time is limited by the arrival of the head of the expansion wave which has been reflected from the driver tube end wall. Hence

it should be possible to increase the test time by increasing the length of the driver tube.

On the basis of the present experiments the equilibrium interface technique appears to be a useful shock tunnel driver technique for increasing enthalpy levels above those obtainable with the tailored interface technique. However it is suggested that further investigation be performed to determine the following:

1. Why the equilibrium pressure correlates with the driver initial pressure and whether this is a general result.
2. The uniformity of the gas that has been processed by the equilibrium interface technique.

REFERENCES

1. Wittliff, C. E. and M. R. Wilson: Shock Tube Driver Techniques and Attenuation Measurements. Cornell Aeronautical Laboratory, Inc., Report No. AD-1052-A-4, August, 1957.

2. Wittliff, C. E.; M. R. Wilson; and A. Hertzberg: The Tailored-Interface Hypersonic Shock Tunnel. Journal of the Aero/Space Sciences, Vol. 26, No. 4, pp. 219-228, April, 1959.

3. Resler, E. L.; S. C. Lin; and A. Kantrowitz: The Production of High Temperature Gases in Shock Tubes. Journal of Applied Physics, Vol. 23, No. 12, pp. 1390-1399, December, 1952.

4. Evans, Robert C.: Operation and Performance of a Shock Tube with Heated Driver. Guggenheim Aeronautical Laboratory, California Institute of Technology, Hypersonic Research Project Memorandum No. 48, February 1, 1959.

5. Hertzberg, A.; W. E. Smith; H. S. Glick; and W. Squire: Modification of the Shock Tube for the Generation of Hypersonic Flow. AEDC-TN-55-15, March, 1955.

6. Glass, I. I.; W. Martin; and G. N. Patterson: A Theoretical and Experimental Study of the Shock Tube. Institute of Aerophysics, University of Toronto, UTIA Report No. 2, November, 1953.

7. Lukasiewicz, J.: Shock Tube Theory and Applications. National Aeronautical Establishment of Canada, Report 15, 1952.

8. Rudinger, G.: Wave Diagrams for Nonsteady Flow in Ducts. New York, Van Nostrand, 1955.

9. Rabinowicz, J.: Aerodynamic Studies in the Shock Tube. Guggenheim Aeronautical Laboratory, California Institute of Technology, Hypersonic Research Project, Memorandum No. 38, June, 1957.

10. Mark, H.: The Interaction of a Reflected Shock Wave with the Boundary Layer in a Shock Tube. NACA TM 1418, 1957.

11. Rabinowicz, J.; M. E. Jessey; and C. A. Bartsch: Resistance Thermometer for Transient High Temperature Studies. Journal of Applied Physics, Vol. 27, No. 1, pp. 97-98, January, 1956.

12. Holder, D. W. and D. L. Schultz: On the Flow in a Reflected-Shock Tunnel. Aeronautical Research Council 22, 152, August 29, 1960.

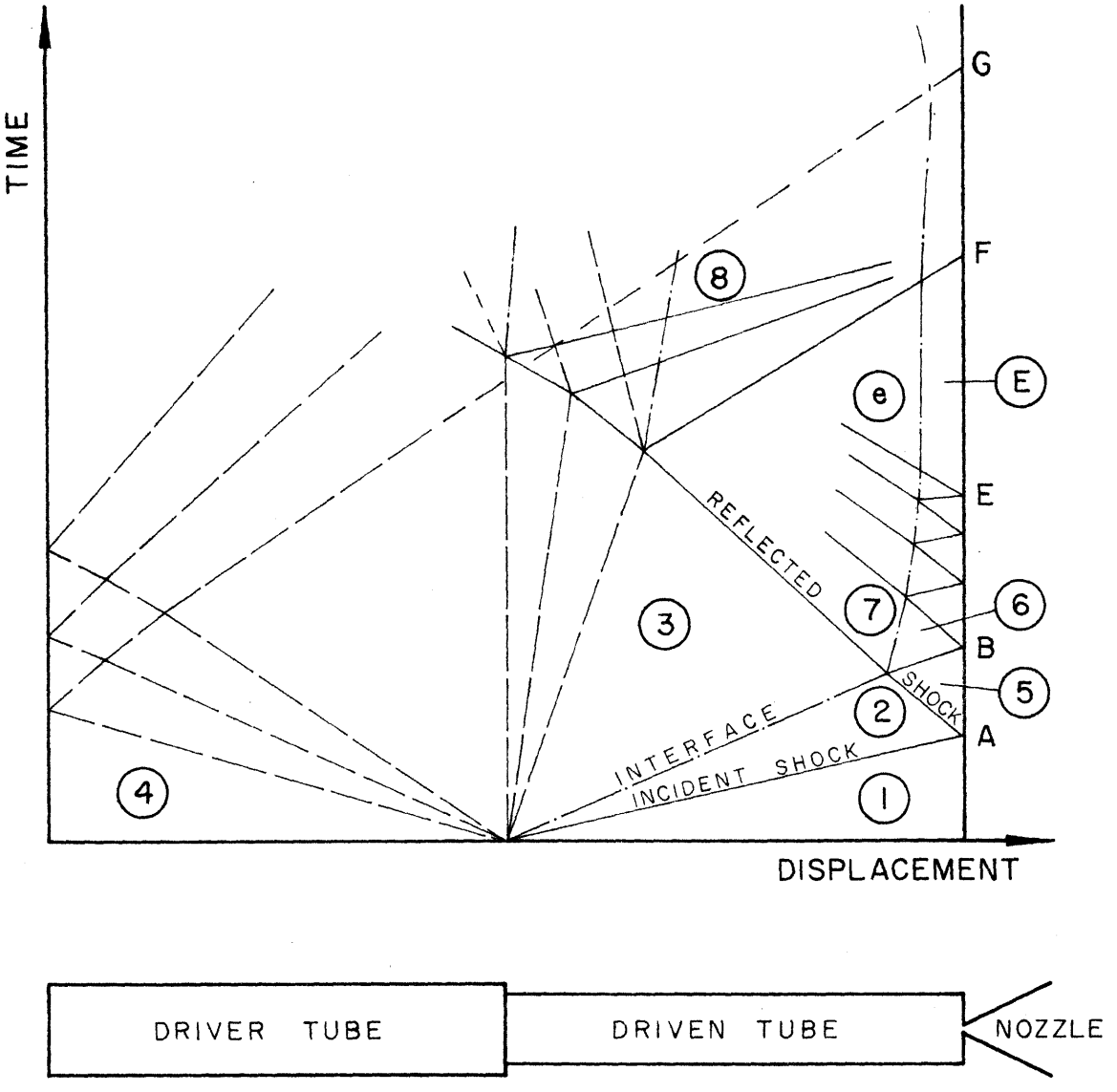

FIG. 1 SHOCK TUNNEL SCHEMATIC AND TYPICAL WAVE DIAGRAM

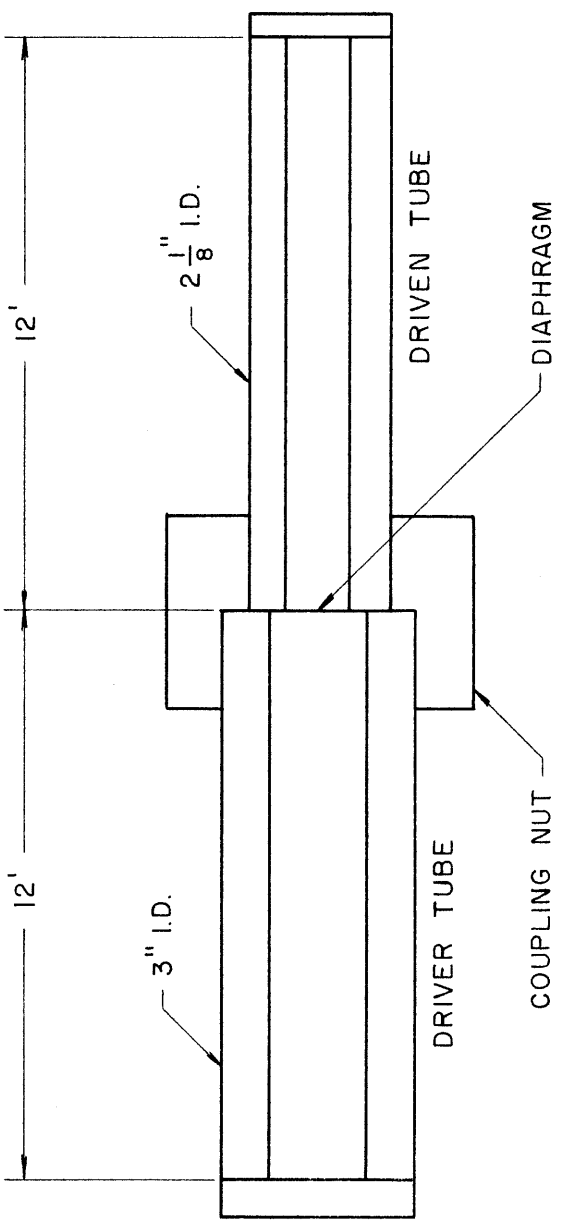

FIG. 2 SCHEMATIC DIAGRAM OF SHOCK TUBE

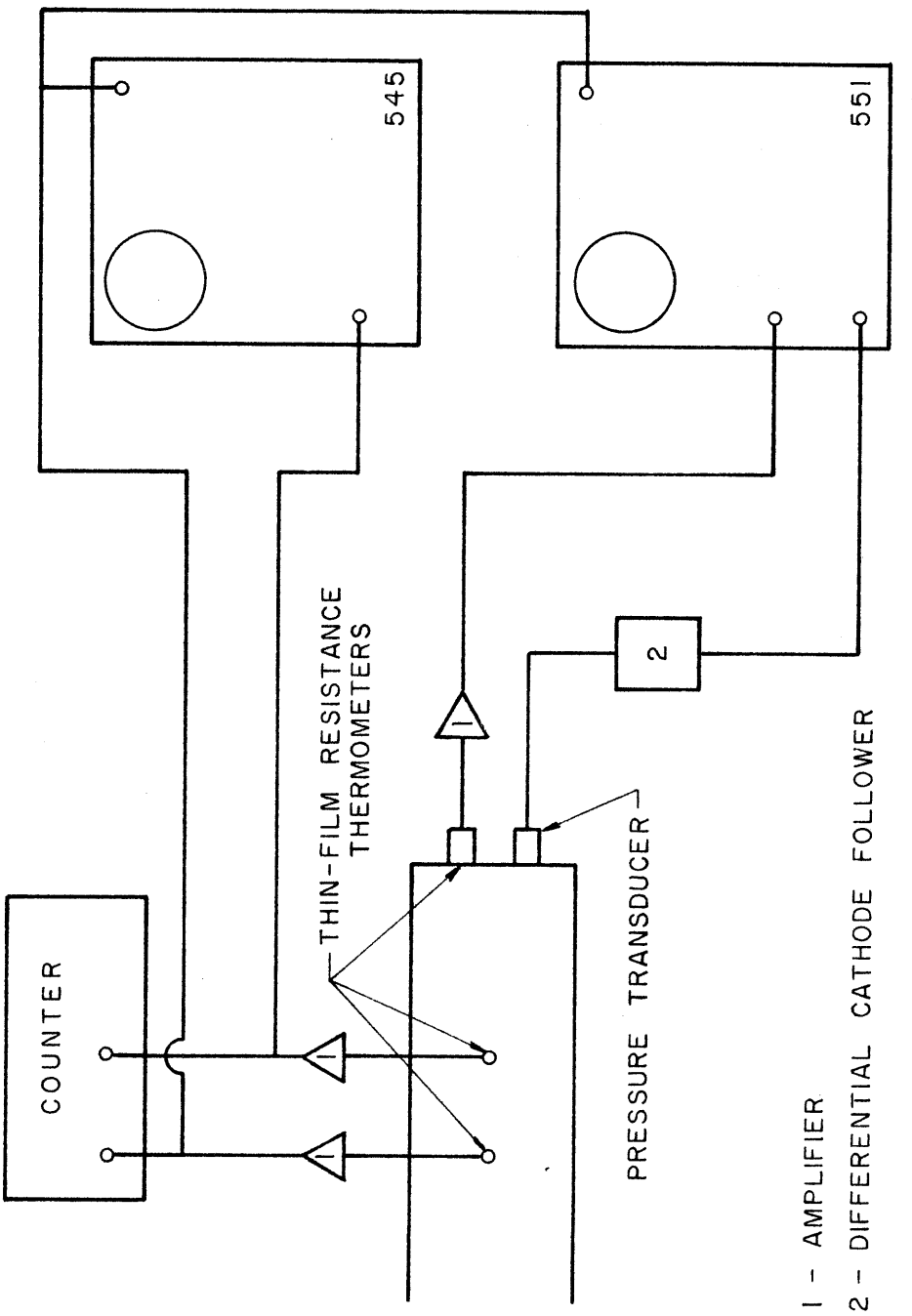

FIG. 3 INSTRUMENTATION BLOCK DIAGRAM

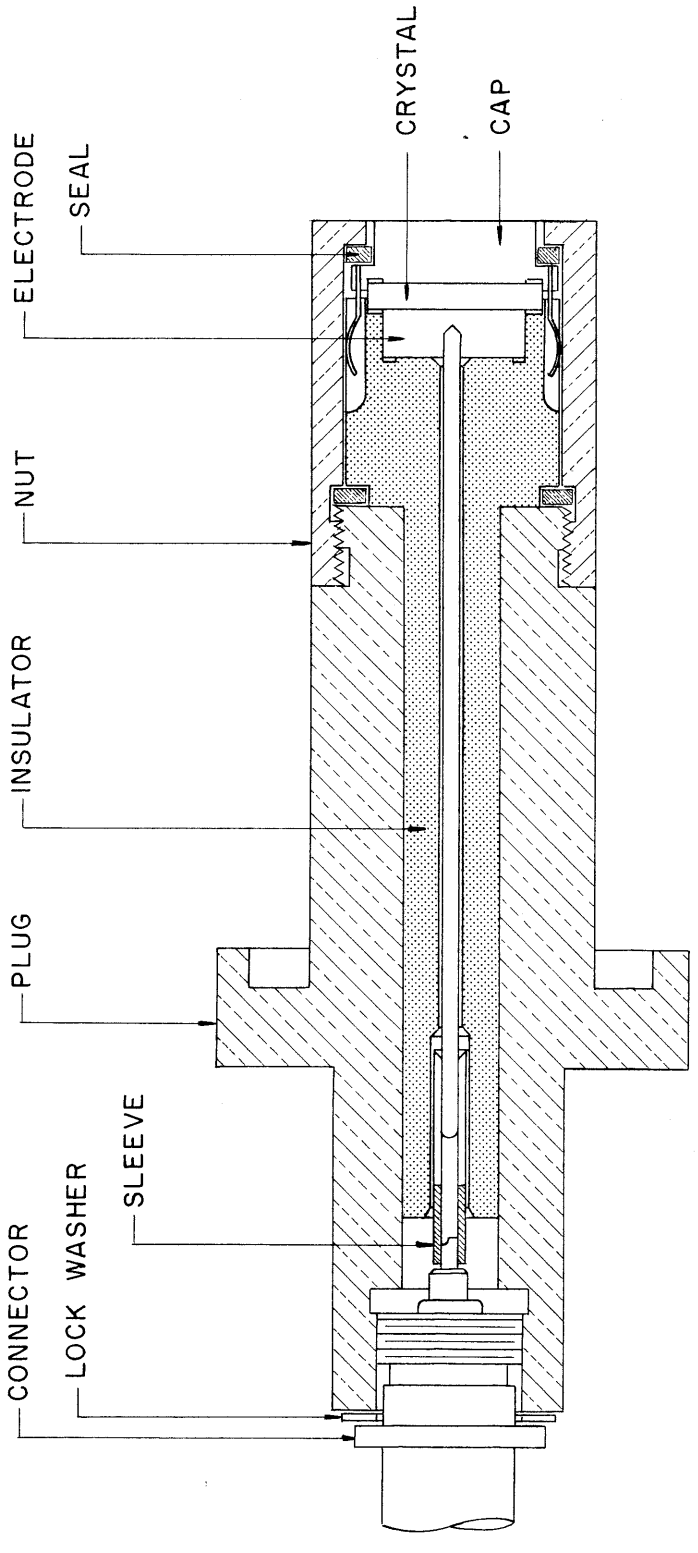

FIG. 4 PRESSURE TRANSDUCER

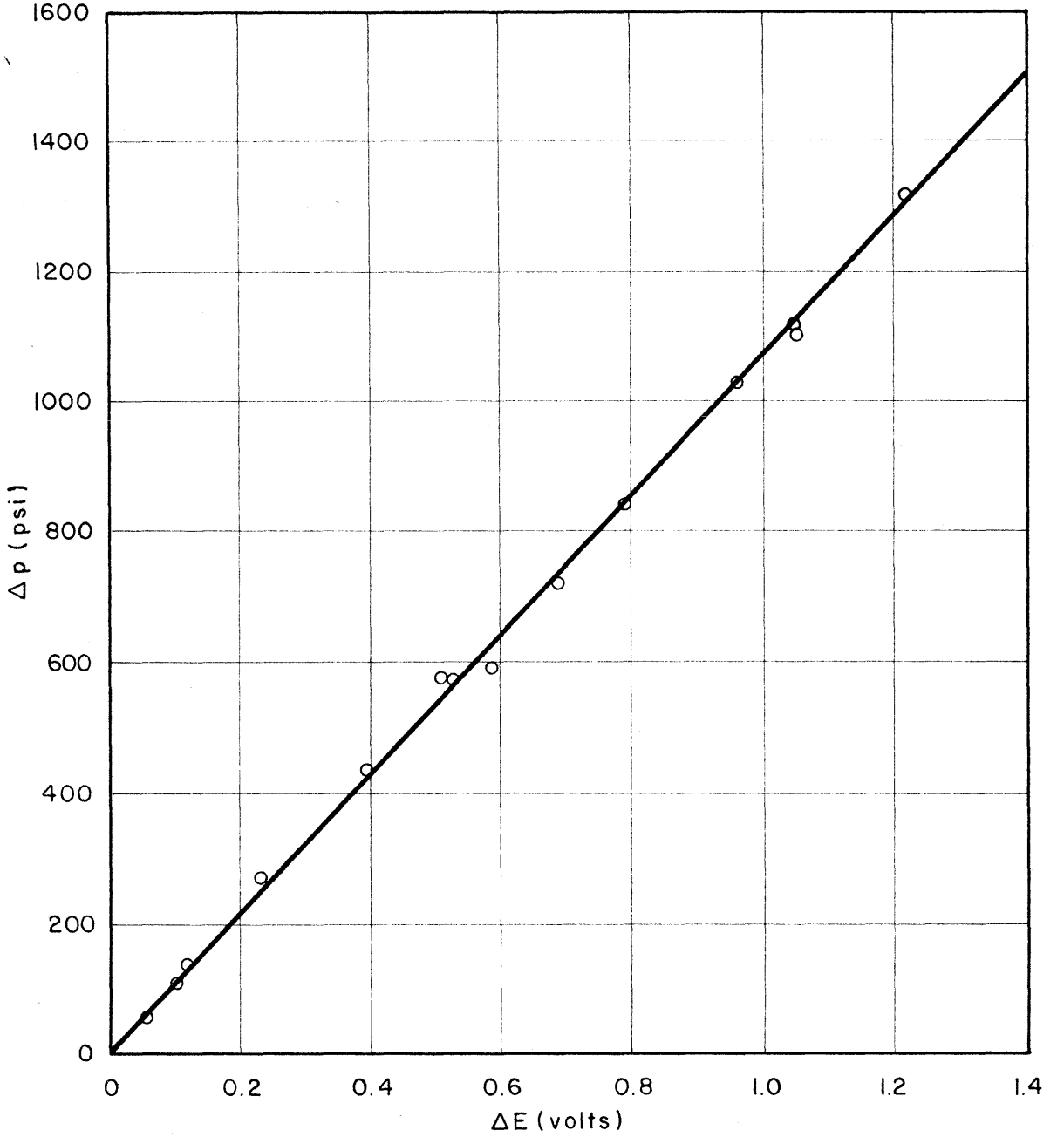

FIG. 5 TYPICAL PRESSURE TRANSDUCER CALIBRATION

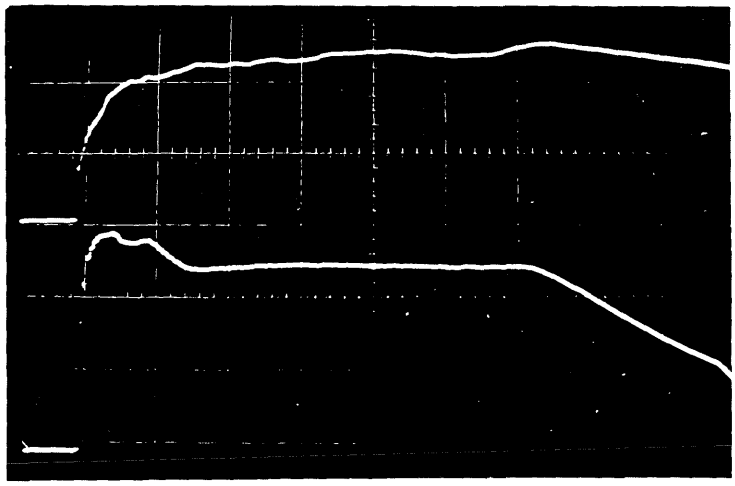

Fig. 6(a). Sweep = 1.0 m sec./div.

M_{S_1} = 3.30; p_1 = 5.01 psia; p_4 = 280 psig

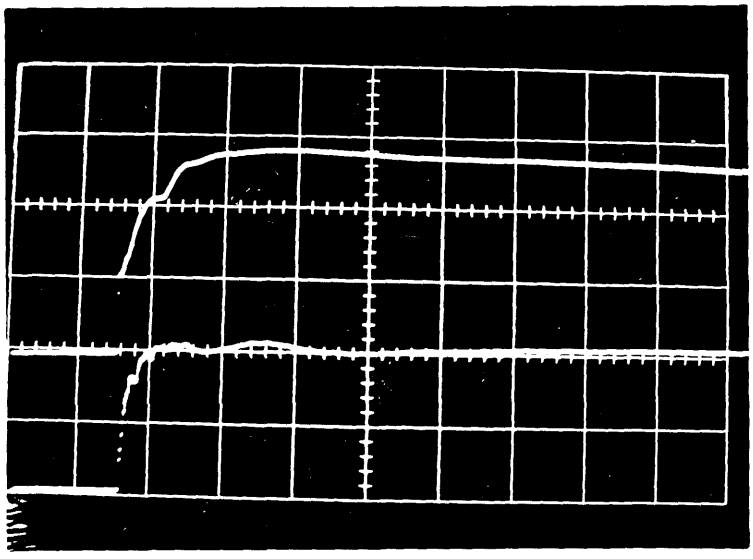

Fig. 6(b). Sweep = 0.5 m sec./div.

M_{S_1} = 3.58; p_1 = 4.98 psia; p_4 = 410 psig

The lower trace is the pressure transducer output.

FIG. 6. RECORDS OF THE PRESSURE AT THE DRIVEN TUBE END

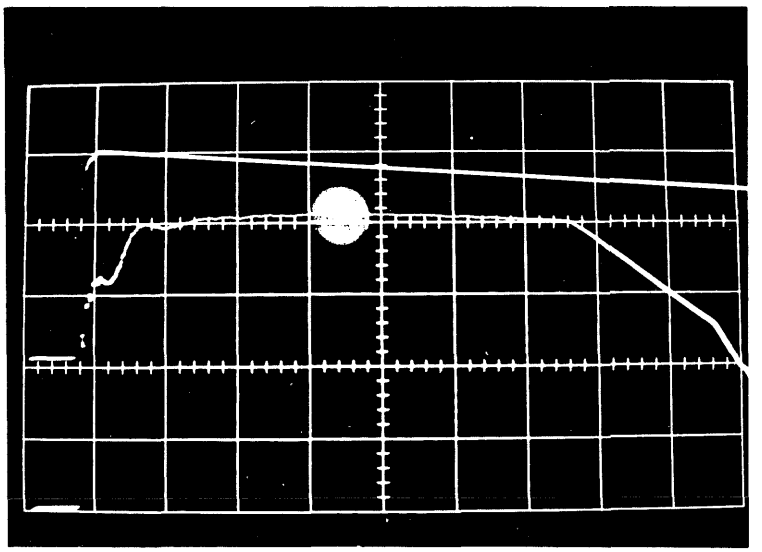

Fig. 6(c). Sweep = 1.0 m sec./div.

M_{S_1} = 4.16; p_1 = 5.02 psia; p_4 = 790 psig

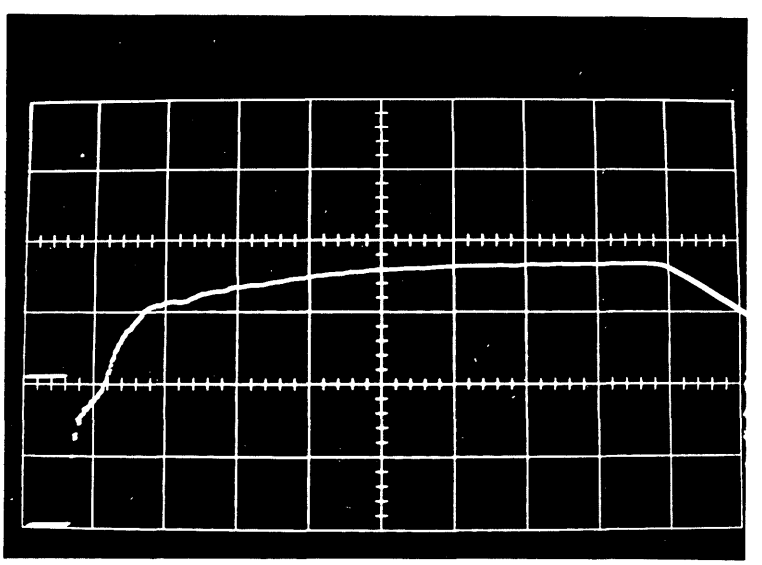

Fig. 6(d). Sweep = 1.0 m sec./div.

M_{S_1} = 4.47; p_1 = 5.06 psia: p_4 = 1830 psig

The lower trace is the pressure transducer output.

FIG. 6 CONTINUED

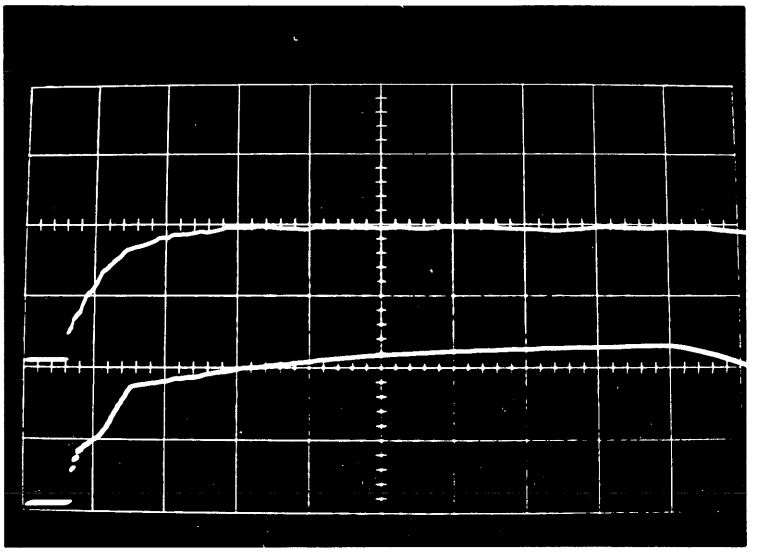

Fig. 6(e). Sweep = 1.0 m sec./div.

M_{S_1} = 4.50; p_1 = 5.03 psia; p_4 = 2130 psig

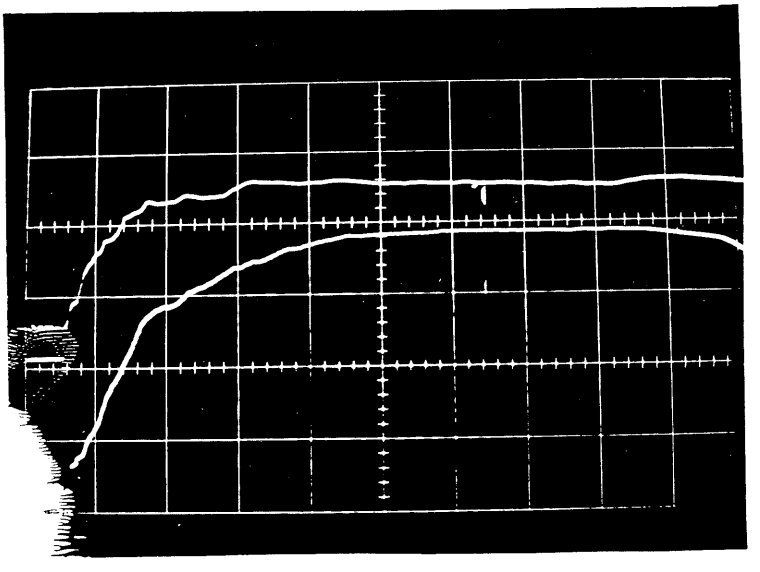

Fig. 6(f). Sweep = 1.0 m sec./div.

M_{S_1} = 4.98; p_1 = 0.966 psia; p_4 = 720 psig

The lower trace is the pressure transducer output.

FIG. 6 CONTINUED

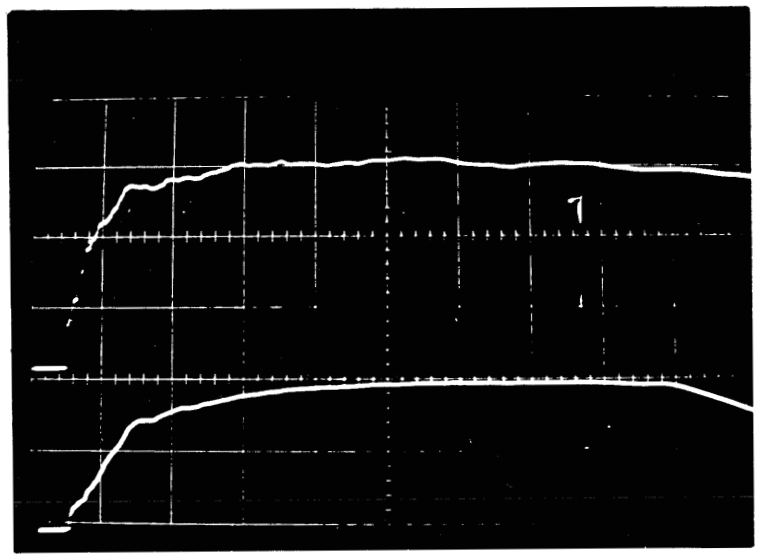

Fig. 6(g). Sweep = 1.0 m sec./div.

M_{S_1} = 5.64; p_1 = 1.003 psia; p_4 = 1000 psig

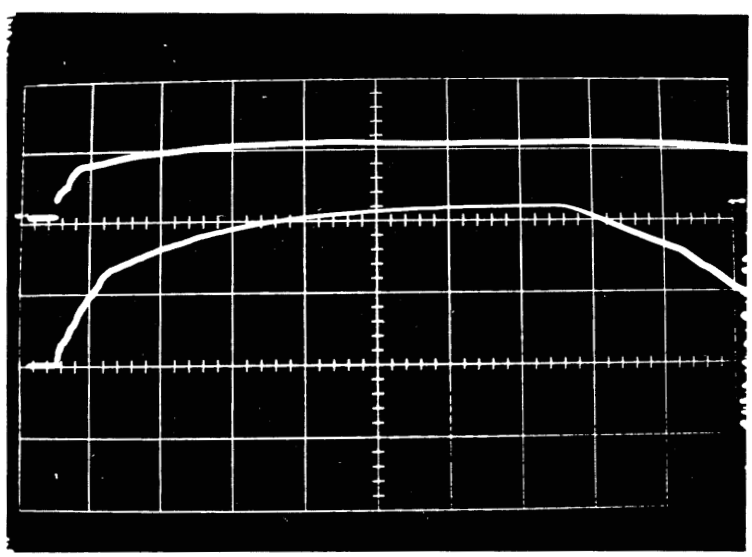

Fig. 6(h). Sweep = 1.0 m sec/div.

M_{S_1} = 6.60; p_1 = 0.975 psia; p_4 = 2550 psig

The lower trace is the pressure transducer output.

FIG. 6 CONCLUDED

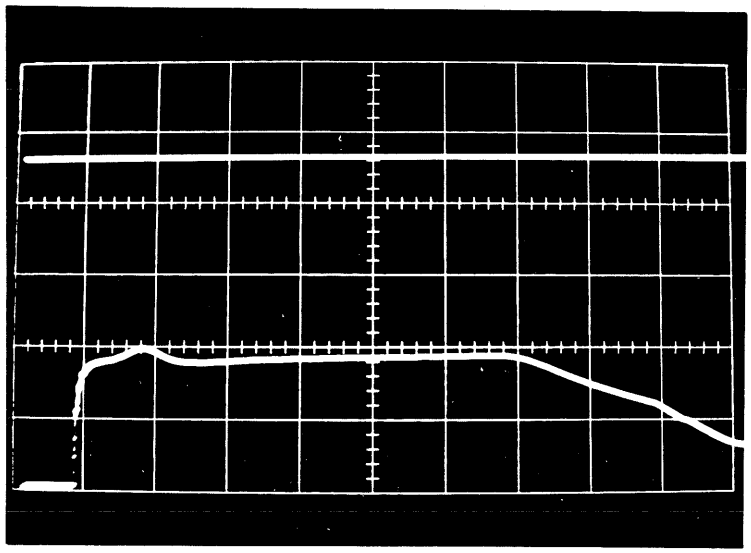

Fig. 7(a). Driven gas: Argon; Sweep = 1.0 m sec./div.

M_{S_1} = 3.84; p_1 = 25.03 psia; p_4 = 2200 psig

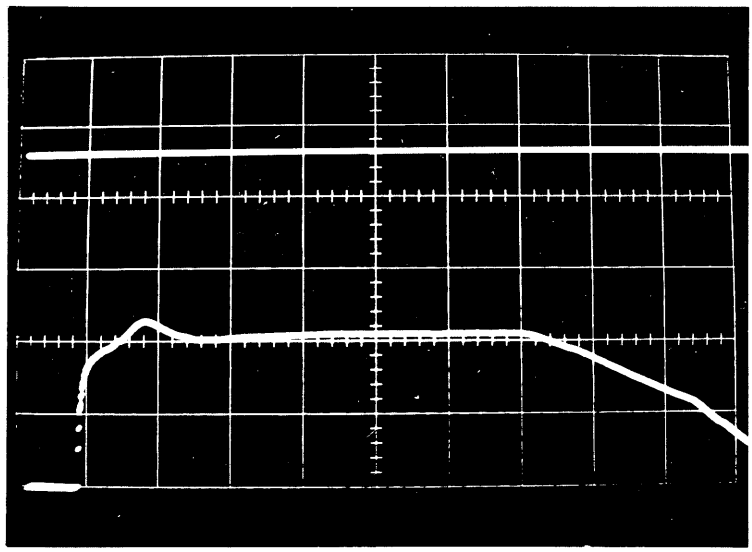

Fig. 7(b). Driven gas: Argon; Sweep = 1.0 m sec./div.

M_{S_1} = 3.92; p_1 = 1.05 psia; p_4 = 75 psig

The lower trace is the output of the pressure transducer.

FIG. 7. PRESSURE RECORDS WITH ARGON AS THE DRIVEN GAS

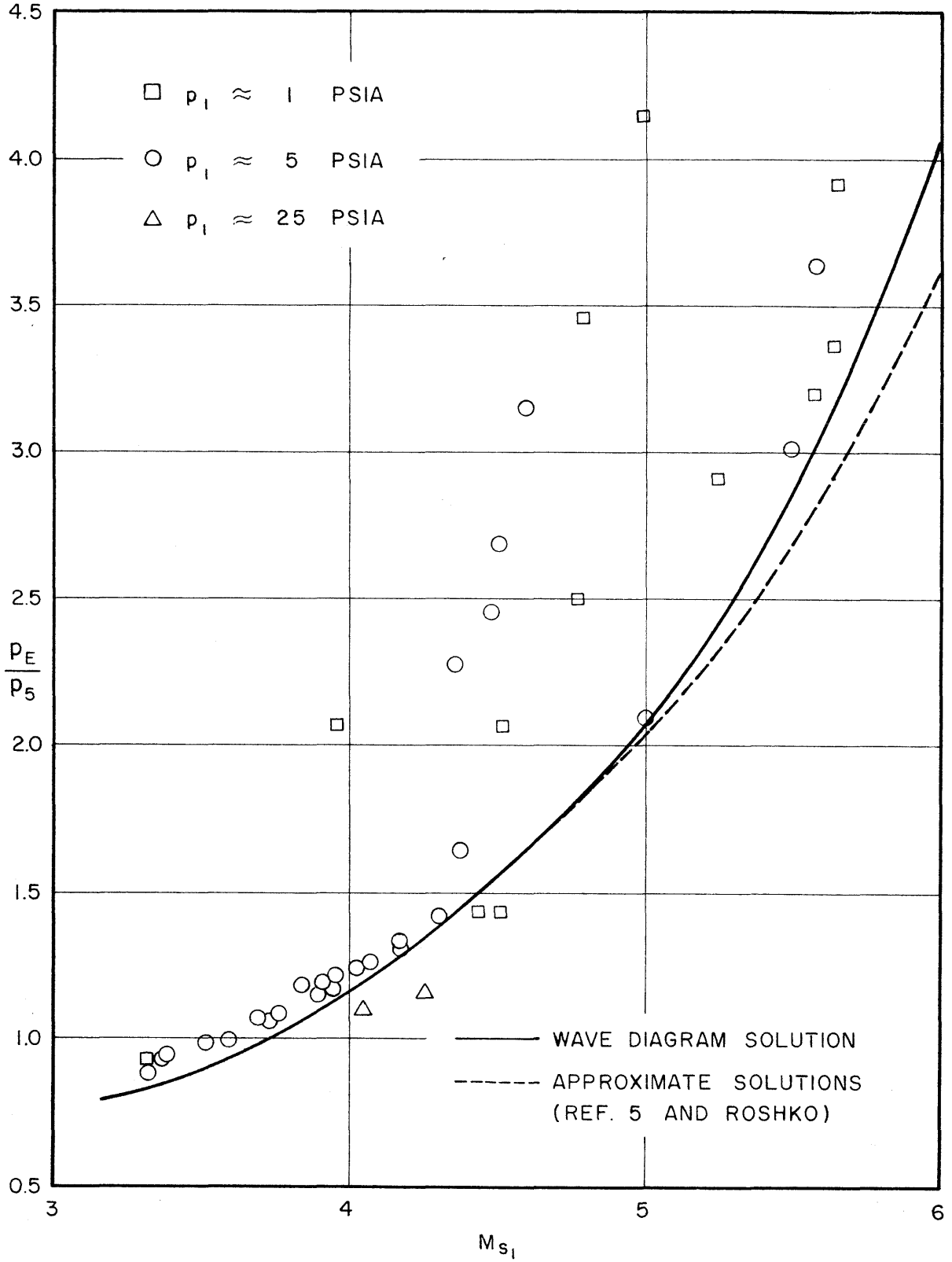

FIG. 8 COMPARISON OF EQUILIBRIUM PRESSURE WITH THEORY

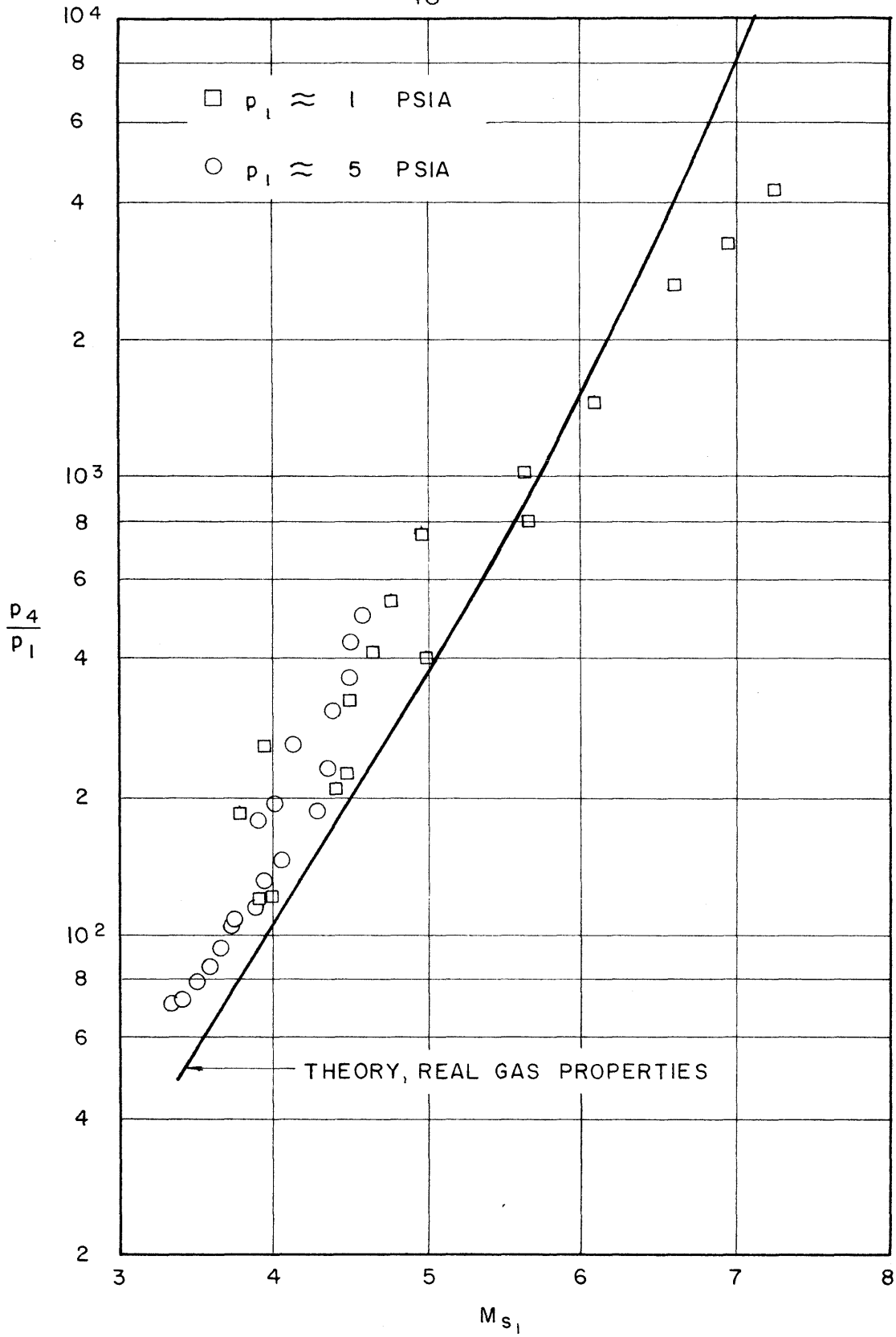

FIG. 9 COMPARISON OF THEORETICAL AND EXPERIMENTAL SHOCK WAVE STRENGTHS

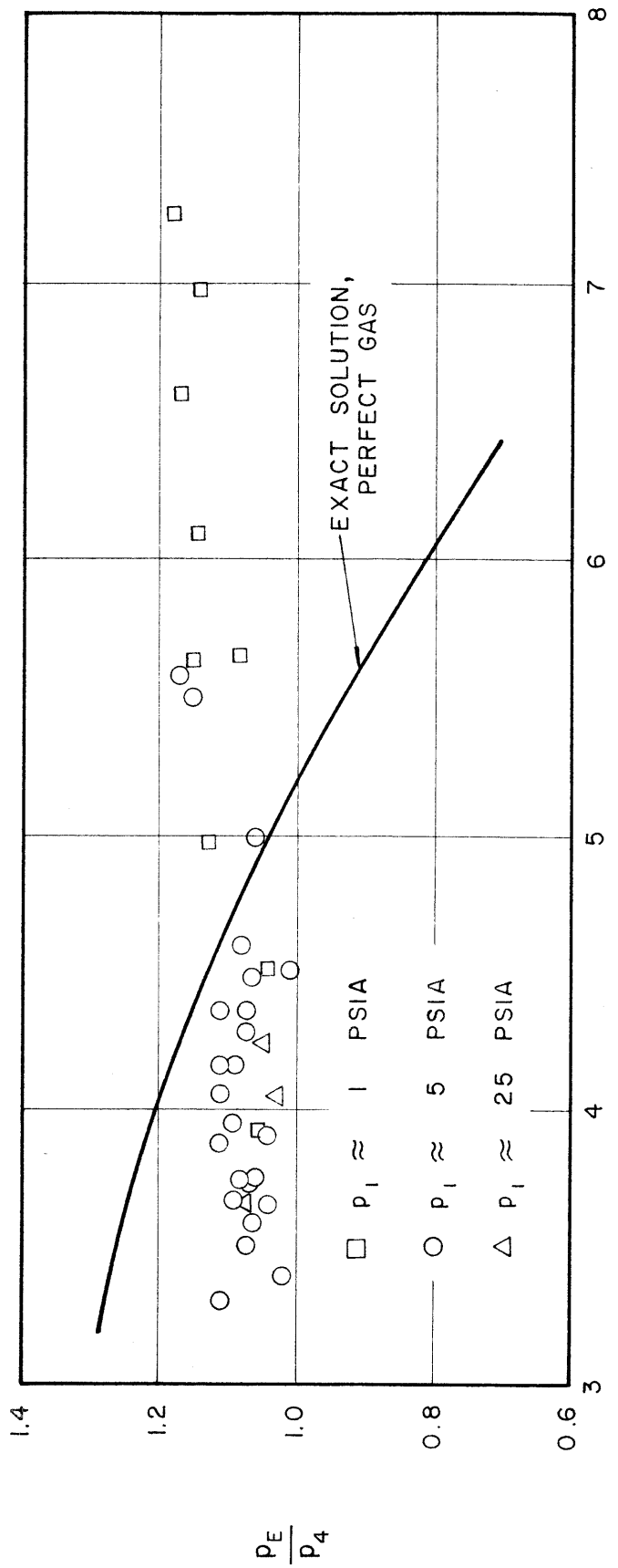

FIG. 10 EQUILIBRIUM TO DRIVER PRESSURE RATIO VS. SHOCK MACH NUMBER

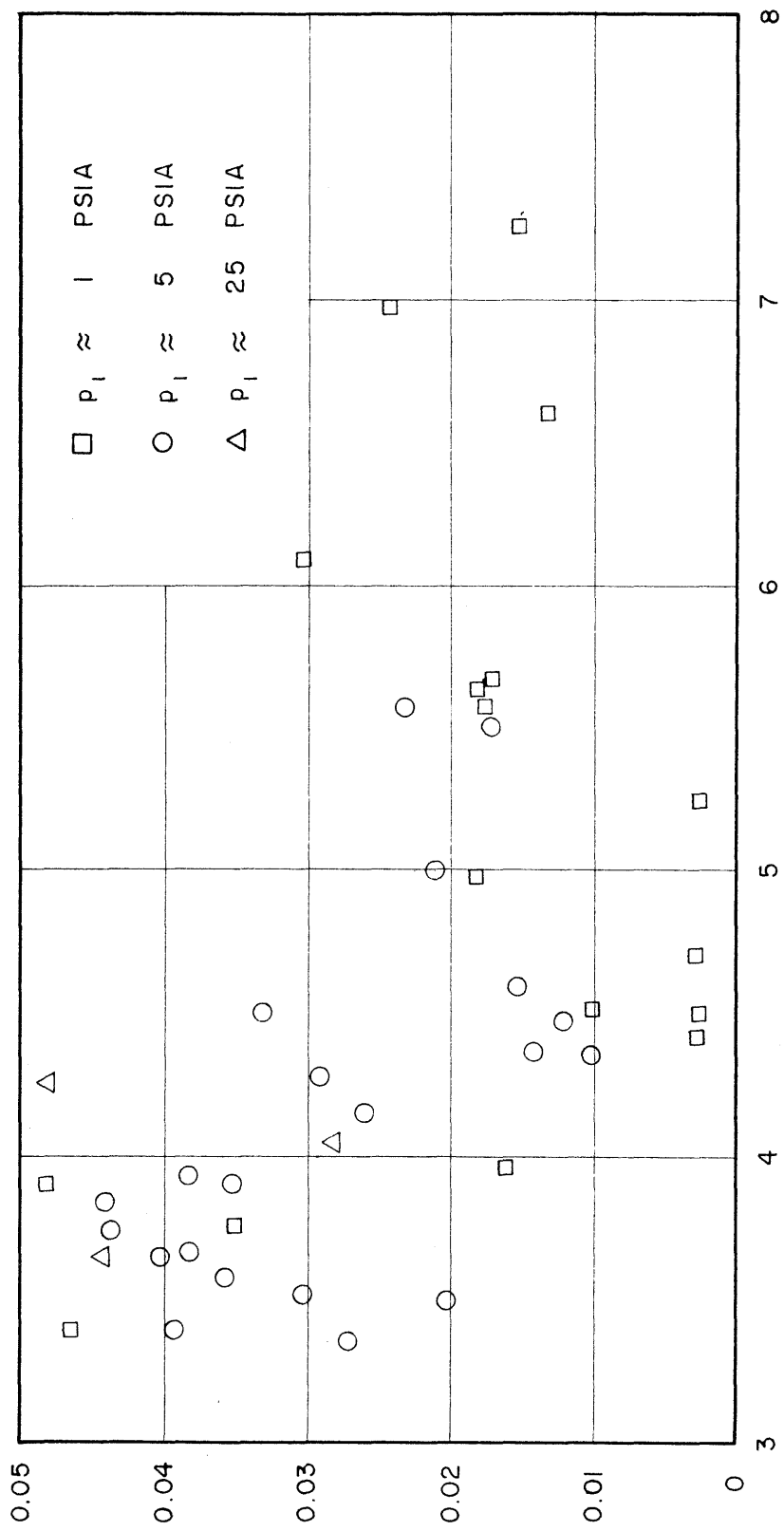

FIG. 11 EQUILIBRIUM PRESSURE VARIATION DURING TEST TIME

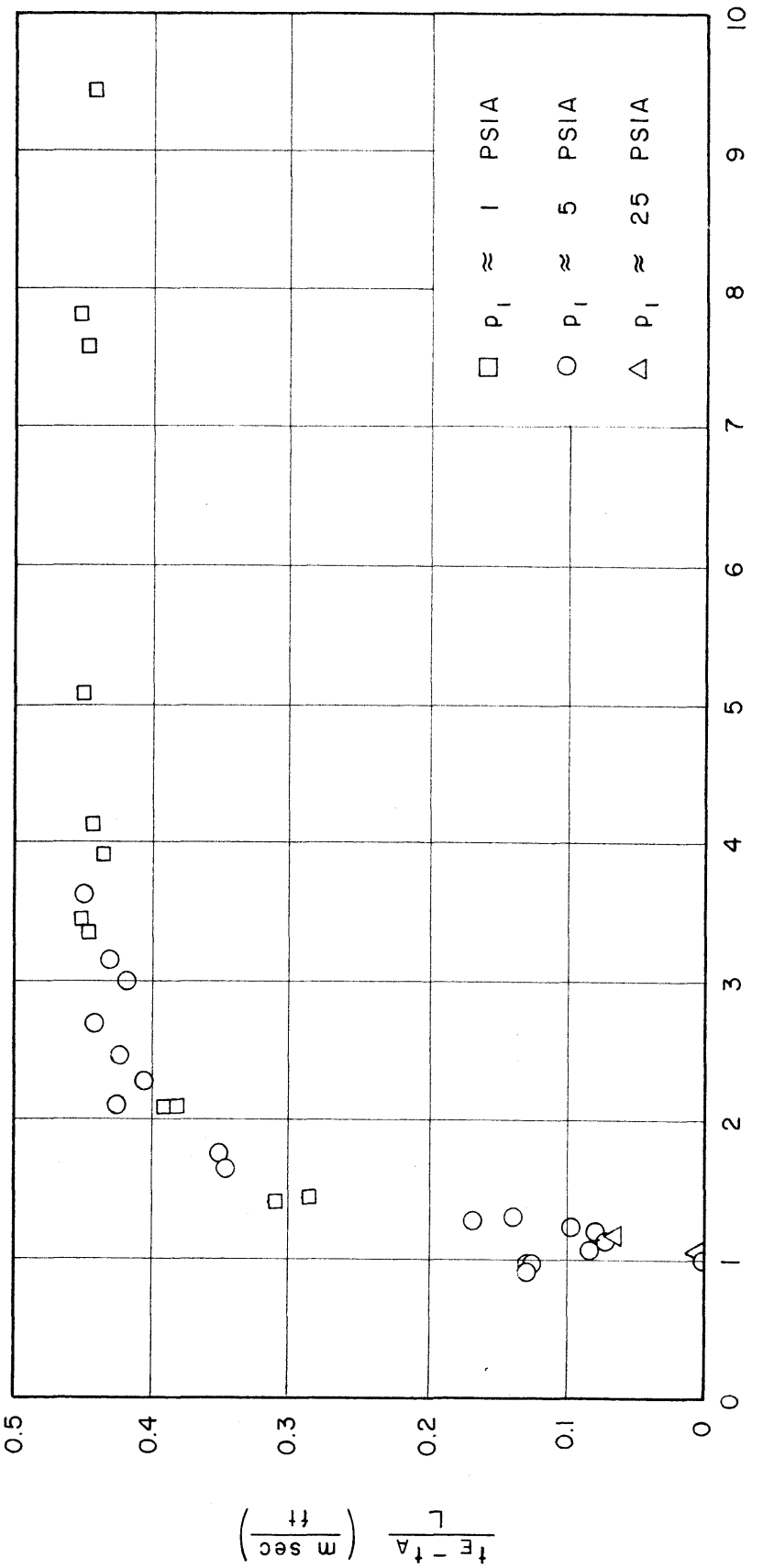

FIG. 12 TIME TO REACH EQUILIBRIUM

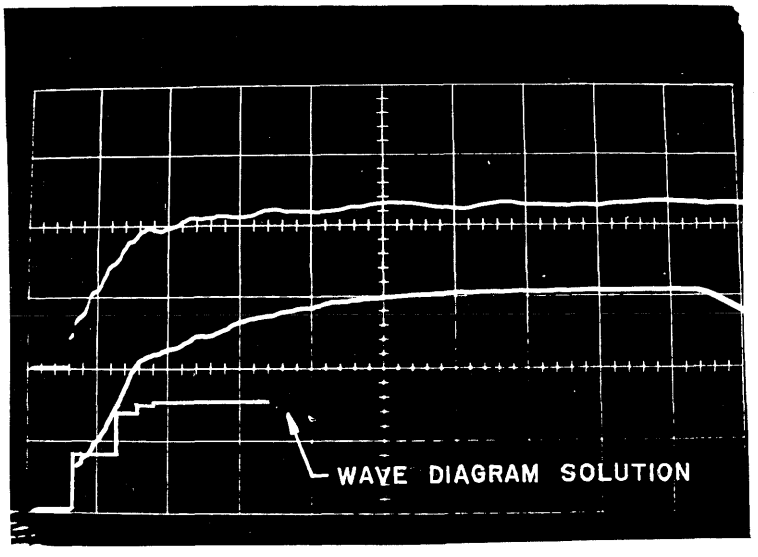

Driven gas: Air; Sweep = 1.0 m sec./div.

M_{S_1} = 4.79; p_1 = 0.994 psia; p_4 = 510 psig

The lower oscilloscope trace is the output of the pressure transducer.

FIG. 13. COMPARISON OF THE ACTUAL AND THEORETICAL PRESSURE HISTORIES AT THE DRIVEN TUBE END WALL

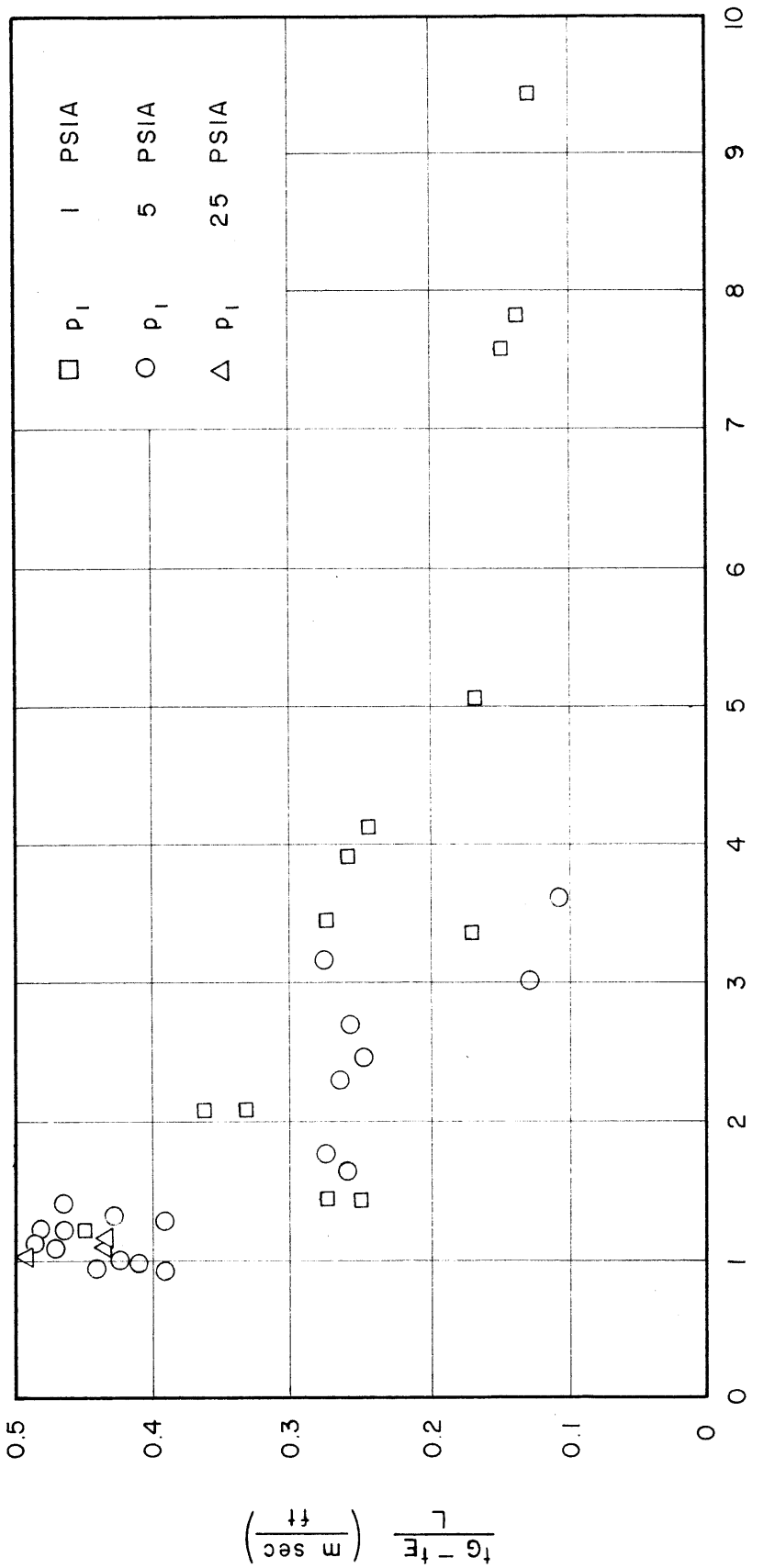

FIG. 14 TEST TIME USING EQUILIBRIUM INTERFACE TECHNIQUE

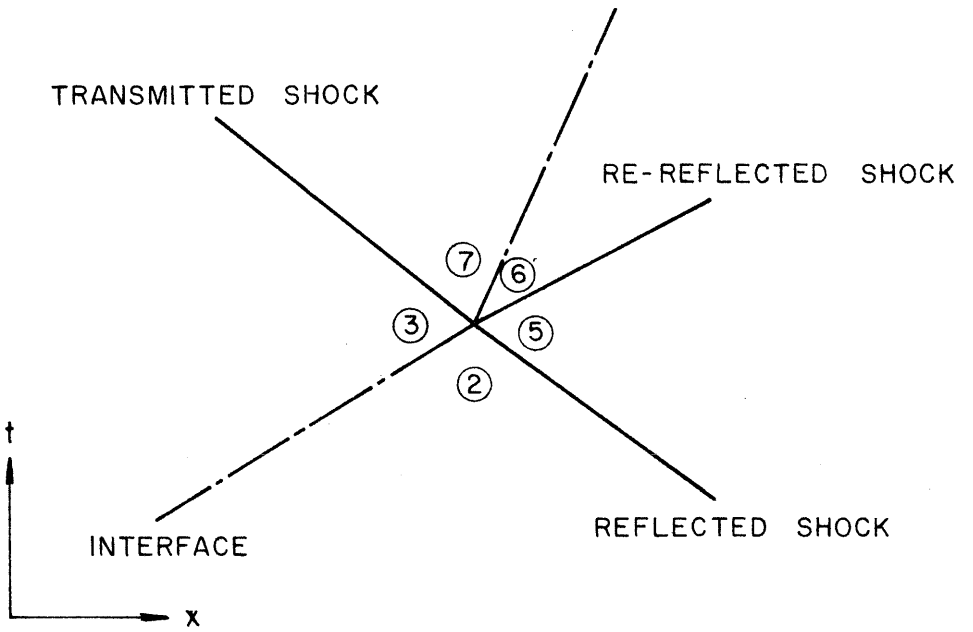

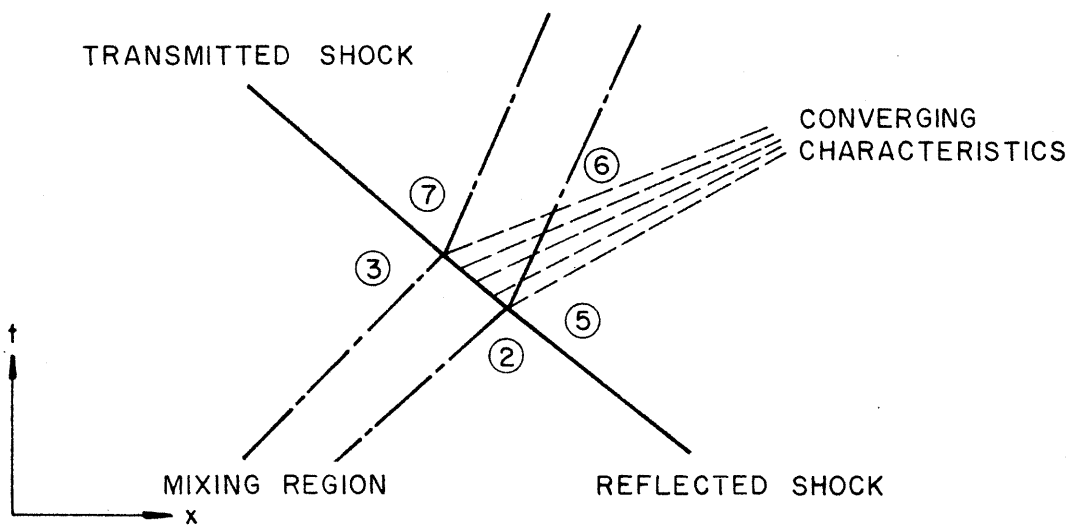

FIG. 15 INTERACTIONS ON THE WAVE DIAGRAM